# Titanium nitride polyaniline bilayer coating for metallic bipolar plates used in polymer electrolyte fuel cells

Cooper, Liam; El-Kharouf, Ahmad

*DOI:*
10.1002/fuce.201900200



*Document Version*
Publisher's PDF, also known as Version of record

*Citation for published version (Harvard):*
Cooper, L & El-Kharouf, A 2020, 'Titanium nitride polyaniline bilayer coating for metallic bipolar plates used in polymer electrolyte fuel cells', *Fuel Cells*. https://doi.org/10.1002/fuce.201900200

DOI: 10.1002/fuce.201900200





# Titanium Nitride Polyaniline Bilayer Coating for Metallic Bipolar Plates used in Polymer Electrolyte Fuel Cells▲

L. Cooper[1]*, A. El-Kharouf[1]

[1] Centre for Fuel Cell and Hydrogen Research, School of Chemical Engineering, University of Birmingham, B15 2TT, United Kingdom

Received December 05, 2019; accepted January 22, 2020; published online ■■■

## Abstract

Two materials, polyaniline (PANI) and titanium nitride (TiN), used for bipolar plate (BPP) coatings have each shown promise in improving the corrosion resistance and contact resistance, respectively, of metallic bipolar plates. Polyaniline was shown to provide a barrier for the bipolar plate and to effectively lower the corrosion currents observed in *ex situ* corrosion tests. However, the interfacial contact resistance (ICR) between polyaniline coatings and gas diffusion layer (GDL) is high and results in high electrical losses. On the other hand, TiN is reported to achieve good conductivity and in some cases improved corrosion resistance.

The two materials have also been investigated together in a composite coating and showed promising results, but the contact resistance of the coating was still too high for use in a commercial fuel cell. In this study, the application of an additional layer of TiN over the TiN-polyaniline composite coating (a bilayer coating) is investigated. Composite bilayered PANI TiN coatings were deposited upon SS316L substrates. The optimized coating achieved U.S. Department of Energy (DoE) targets with potentiostatic corrosion currents of ~0.024 $\mu A\,cm^{-2}$ and ICR values of 11.2 $m\Omega\,cm^2$. PANI polymerization was confirmed, using Fourier-transform infrared (FTIR) spectroscopy and TiN loadings were investigated with energy dispersive X-ray (EDX) spectroscopy .

**Keywords:** Bipolar Plate, Coating, Composite Layer, Composite Polymers, Polyaniline, Polymer Electrolyte Fuel Cell, Titanium Nitride

## 1 Introduction

Transportation accounts for 14% of all greenhouse gas emissions on the planet; new renewable technologies for use in the transportation sector are being investigated at ever increasing rates in the hope of stifling carbon emissions [1]. Vehicles powered by hydrogen in an electrolytic fuel cell are one option to prevent the carbon emissions of vehicles. Hydrogen fuel cells produce a DC electrical current by electrochemically reacting gaseous hydrogen with air or more specifically oxygen [2]. A hydrogen fuel cell stack is comprised of many individual fuel cells connected in series *via* bipolar plates (BPPs). BBPs provide structural support for the cell, electrical conduction for the electrons, deliver the reactant gases to the cell and remove the produced water out of the cell. BPPs have also been used to aid in heat rejection from the cell, whereby intermittent cells in a stack can be machined with cooling channels. Both the GDL and BPP work to remove the produced water from the cell, as poor removal of water can lead to flooding which reduces the cell's performance and efficiency. BPPs account for about 80% of the weight, most the volume and 45% of the total cost of a PEFC stack, making cost reduction of BPP essential for commercial viability [3–5].

Traditionally, BPPs have been made from high density graphite. Graphite provides excellent corrosion resistance and has a very low interfacial contact resistance with the carbon paper used as GDL. However, graphite is costly to process and machine, it is brittle and thick plates are required to provide the necessary mechanical requirements of the stack [6]. Researches are searching for potential replacements for graphitic plates with metallic substrates being readily investigated. Stainless steels and other metallic materials, such as

▲ *Paper presented at the 23rd EFCF Conference "Low-Temperature Fuel Cells, Electrolyzers, H2-Processing Forum" (EFCF2019), 2–5 July 2019 held in Lucerne, Switzerland. Organized by the European Fuel Cell Forum www.efcf.com*

[*] *Corresponding author, ltc733@.bham.ac.uk*

aluminium and titanium, have seen much research due to their superior properties in terms of material costs, manufacturability, mechanical properties and electrical conductivity [7, 8]. The use of metallic materials allows for the production of thinner plates, thereby improving the volumetric power density of the fuel cell stack [6, 9]. Metallic BPPs also have good thermal conductivity which is essential for the thermal management of high power stacks [10, 11].

However, metallic plates do suffer in the high potentials and acidic environment found in polymer electrolyte fue cells (PEFCs) (pH of 3.4 and transient potentials reaching 0.8 V [12]). A passive oxide layer forms on the surface of the stainless steel in the presence of oxygen, which although offers additional corrosion protection in aggressive environments [13], and it causes the contact resistance to greatly increase, reducing the performance of the stack. For this reason, coatings for metallic bipolar plates that provide an effective barrier to the harsh conditions have seen extensive research. Moreover, coatings need to achieve and maintain a low contact resistance as to avoid electrical losses in the stack. BPPs are expected to have an ICR of less than 10 $m\Omega\,cm^2$ and cathodic corrosion resistances of less than 1 $\mu A\,cm^{-2}$ according to the DoE 2020 targets [2]. Coatings of SS plates need to achieve these performance targets, if PEFC stacks are to be commercially viable.

As metallic BPPs alone do not satisfy DOE targets, research has focused on coating development to improve both the corrosion properties and interfacial contact resistance. Many different techniques exist for applying coatings, including: (i) physical vapour deposition (PVD), (ii) chemical vapour deposition (CVD), (iii) electroplating and electrophoretic deposition [14–17]. When comparing the coating methods in terms of scalability and cost, it can be noted that physical and chemical vapour deposition methods require batch production which could limit mass production and increase cost [18]. Electroplating and electrophoretic deposition are two such techniques which can be used as part of a continuous production line, and both of which can provide uniform coatings on complex shapes [19].

Progress in the development of metallic BPPs by coating them with transition metal nitrides was reported in literature [11, 20, 21]. Metal nitrides, most notably chromium nitride and titanium nitride [21–23], have been investigated, due to their effective corrosion protection and improved interfacial conductivity. Group 4 (periodic table) metal nitrides, namely titanium, are typically used for coatings on cutting tools, due to their hardness and their chemical and thermal stability [24, 25]. Titanium remains metallic in the nitride matrix, due to the electron structure in the metals d-orbital, the metallic structure results in titanium nitride showing good electrical conductivity [25]. Furthermore, the resistance to oxidation results in TiN maintaining its conductivity in the aggressive conditions, such as those found in PEFCs. Deposition of titanium nitride in industry is typically achieved *via* physical vapor deposition (PVD), although other methods involving chemical vapor deposition (CVD), or plasma nitriding are also popular [26]. Pugal Mani coated 316L with TiN, TiAlN and a composite layer of TiN/TiAlN *via* a cathodic arc evaporation system [20]. The TiN sample showed adequate corrosion potentials and low corrosion currents. The TiN also showed the lowest ICR with values around 1 $m\Omega\,cm^2$.

In addition, vast research has been committed to conductive polymers for PEFC BPP coatings, because of their chemical stability and their relatively high conductivity and redox functions [27, 28]. Polymers also offer low cost in terms of application processes and materials. Polyaniline and polypyrrole are two such conductive polymers. Both are chemically stable and researchers have found that polymer coatings can reach corrosion current requirements of PEFCs in *ex situ* corrosion tests, effectively providing a barrier for the BPP [29, 19]. Joseph et al. reported that the increased thickness of the polyaniline coating leads to increased pin hole defects [30]. Thicker coatings also increase the ICR of the samples. Polymer coating can be applied by employing various methods, for instance Joseph et al. painted polyaniline onto the surface of the substrate by dissolving the polyaniline in xylene [31, 32], whereas electrochemical polymerization was used by other researchers to apply the polymer coating [12, 20, 31, 33]. However the interfacial contact resistance between polymer coatings and GDLs is high and results in high electrical losses.

In order to combine the benefits of multiple materials, composite bilayered materials were developed. Zhang et al. chose polyaniline due to its excellent corrosion properties and looked to improve upon its poor conductivity by combining the coating with gold nanoparticles and carboxyl group functionalized carbon nanotubes [34]. The composite coating satisfied DoE corrosion targets and had a much reduced ICR of 16.6 $m\Omega\,cm^2$, thereby showing how the combination of coatings can symbiotically improve the coating. Surbhi et al. also used a polymer coating, which was doped with titanium nitride (TiN) [29]. This coating also produced an effective barrier to corrosion products that satisfied DoE corrosion targets. ICR values of the composite polymer coating were also reduced relative to pure polymer coating.

This work looks to further development of polymer-metallic composite coatings, by optimizing a thin titanium nitride (TiN) polyaniline composite layer using low temperature plating solutions. This was then modified to produce a bilayered coating with an electrodeposited surface layer of TiN. The coatings were characterized to confirm the deposition of PANI and TiN, and then examined for their corrosion resistance and ICR. The aim here is to reduce the ICR achieved in literature to values within the DoE target while maintaining the reported corrosion resistance.

## 2 Experimental

### 2.1 Coating Process

An electroplating three-electrode cell was designed and 3D printed using TinkerCAD software and a MakerBot Replicator 2 FDM printer, respectively. Two platinum mesh counter electrodes were used to get a homogenous coating on both sides

  

of the sample simultaneously. The AISI 316 stainless steel (SS) sample (30 × 50 mm) is placed in the center housing equidistant from the two counter electrodes with the reference electrode fixed to the edge of the cell. The SS sample is the working electrode in the three electrode setup. A silver/silver chloride was used as a reference electrode for this work.

Before coating, the samples were first wiped with ethanol to remove grime off the surface. They are then acid washed in 50% sulfuric acid solution to remove the passivation layer on the SS surface, after 10 min the samples were removed and immersed in deionized water, rinsed and dried under a nitrogen stream.

The coating electrolyte was prepared in a 0.1M sulfuric acid solution. Aniline monomer (Sigma Aldrich) concentration was fixed at 0.1M, and TiN nanoparticles (SkySpring Nanomaterials Inc. (97+% purity and 20 nm particle size)) were added for the composite coating, the loading was set at 0.5 g $L^{-1}$. The solution was sonicated for 10 min and then cooled to a temperature of 5 °C in an ice bath, then shaken by hand, before being used in the plating cell.

Applied potentials were implemented via an IVIUMSTAT.XRi potentiostat. The electropolymerisation of aniline and co-deposition of TiN was achieved by cyclic voltammetry (CV). Static potentials were also used to create a TiN surface layer (in the bilayer coatings). A list of samples and coating parameters are shown in Table 1. For the CV cycles, the potential was swept from –0.18 to +1.00 $V_{Ag/AgCl}$ at a scan rate of 50 mV $s^{-1}$ and a potential step of 5 mV for 5 cycles. After plating, samples were removed from the cell, rinsed with DI water and then dried under a nitrogen stream.

Table 1 Samples and their coating procedure.

| Sample name | CV cycles | Time potential held static at 0.5 V / s |
|---|---|---|
| Bare SS | 0 | 0 |
| PANI | 5 | 0 |
| PANI 150s | 5 | 150s |
| PANI TiN | 5 | 0 |
| PANI TiN 150s | 5 | 150s |
| PANI TiN 300s | 5 | 300s |
| PANI TiN 450s | 5 | 450s |
| PANI TiN 600s | 5 | 600s |
| TIN 600s | 0 | 600s |

Table 2 Samples and their coating procedure.

| Sample name | Potential held static at 0.5V for / s | Titanium loading | |
|---|---|---|---|
| | | Weight % | Atomic % |
| PANI TiN | 0 | 6.87 | 7.63 |
| PANI TiN 150s | 150 | 6.10 | 6.79 |
| PANI TiN 300s | 300 | 5.88 | 6.48 |
| PANI TiN 450s | 450 | 7.11 | 7.71 |
| PANI TiN 600s | 600 | 8.41 | 8.94 |
| TIN 600s | 600 | 7.17 | 7.95 |

### 2.2 Coating Characterization

#### 2.2.1 Fourier-transform Infrared (FTIR)

FTIR spectroscopy measurements were carried out to confirm the electropolymerization of aniline using a Bruker Lumos device in the reflectivity setup. The ATR crystal was wiped clean before every measurement and background scans were carried out using 64 scans on the gold reference plate. For the measurements, 1,000 scans were taken on samples specifically made for the FTIR test. The tested samples were 25 cycle pure polyaniline (25 cycle PANI) and polyaniline titanium nitride (25 cycle PANI TiN) coated SS316L, using the solutions reported in Section 2.1. These were made because the polyaniline coatings deposited with 5 CV cycles for the test samples were too thin and could not be detected using the FTIR device.

#### 2.2.2 Energy Dispersive X-ray (EDX)

EDX measurements were carried out using a JOEL JSM6060LV scanning electron microscope (SEM) equipped with EDX. A 5 kV beam was used to achieve surface measurements to quantify the surface loading of titanium of the samples.

### 2.3 Interfacial Contact Resistance

The ICR measurements were taken between the samples and two gas diffusion layers (Toray 60) following the method described in [29]. An Instron 584 microtester was used to control the compression force on the samples. The carbon paper GDLs are pre-cycled by compressing to 300 N $cm^{-2}$ between two gold plated copper pins with a surface area of 1$cm^2$ and then cycling between 250 N and 300 N for 2 h at a rate of 50 N $s^{-1}$. Pre-cycling is conducted as the GDLs have irregular compressible behavior which can alter the measured ICR values [35].

SS samples are placed between two pre-cycled GDLs, this is then loaded onto the microtester between the two plated pins. The samples are then compressed from 20 to 300 N in 20 N steps, with each value being held for 30 s as to allow the resistance value to stabilize. The resistance is measured by a precision Milli/Micro-Ohmeter. The ICR value is then calculated from the overall measured resistance as explained in [29]. The ICR was measured for the samples before and after the corrosion test to assess the stability of the coating.

### 2.4 Electrochemical Corrosion

Metal samples were loaded into the corrosion three-electrode electrochemical cell with a sample exposed area of 1 $cm^2$. A pH3 sulfuric acid solution is used as an electrolyte and the cell temperature was maintained at 80 °C to simulate the PEFC environment. Reference and counter electrodes of mercury/mercury sulfate (MSE) and platinum mesh, respectively, were used. The cell was then connected to the potentio-

  

Table 3 Potentiostatic corrosion current at 0.9$V_{SHE}$.

| Sample | Corrosion current density / nA $cm^{-2}$ |
|---|---|
| Bare SS | 31.677 |
| PANI | 62.116 |
| PANI TiN | 48.080 |
| PANI TiN 600s | 22.754 |
| TiN 600s | 21.802 |

stat (IVIUM compactstat). A potentiodynamic test was then carried out in nitrogen atmosphere by means of linear sweep voltammetry; sweeping the potential from –0.5 to 1 $V_{SHE}$ at a sweep rate of 10 mV $s^{-1}$ for 11 cycles. This experiment was then repeated after the potentiostatic corrosion test. After the LSV the gas line was swapped to bubble the solution with air for 20 min in preparation for the potentiostatic corrosion test. Amperometric detection was used to hold a constant potential of 0.9 $V_{SHE}$ for 24 h.

## 3 Results and Discussion

### 3.1 Coating and Characterization

Polyaniline was coated onto the SS316L substrates *via* a 5 cycle cyclic voltammetry (CV). Thin 5 cycle coatings have been shown to minimize the ICR and porosity of polyaniline coatings [29]. The reduced porosity enhances the corrosion resistance of polyaniline coatings. Previous work showed thicker coatings cause a more porous structure [20]. By controlling the temperature and initiating electroplating experiments at 5 °C, thinner coatings can be achieved. The CV scans carried out at 5 °C did not show the traditional peaks seen in electropolymerization of aniline. Figure 1a shows the CV cycles produced in a solution of 0.1 g $L^{-1}$ TiN and 0.1M aniline at 25 °C. The peaks observed here are due to the higher number of reactions occurring at the elevated. This shows that polymerization of the aniline was successful in the chosen potential window and under the specified conditions. It is likely that the peaks were not observed at 5 °C, because the current flowing was minimal. Three redox peaks can be seen within the CV potential window (–0.18 and 1 $V_{SHE}$) for the forward and reverse scan. These peaks show the change in oxidation state of the polymerized aniline monomer. Formation of the desired conductive emeraldine oxidation state corresponds to the peak observed between 0.4 to 0.5 $V_{SHE}$. No clear peak can be seen for the electrodeposition of TiN, however during CV scans deposition of TiN and polymerization of aniline have been reported [29]. It is possible that the TiN gets trapped in the structure as the aniline polymerizes. Another possible mechanism could be the TiN electrophoretically depositing at sites across the PANI surface, claiming nucleation sites and slowing the polymerization of the PANI. The surface layer of TiN was achieved *via* holding a static potential of 0.5V.

Figure 1b shows the FTIR spectrum of the 25 cycle PANI and 25 cycle PANI TiN. The intensity of the peaks is indicative

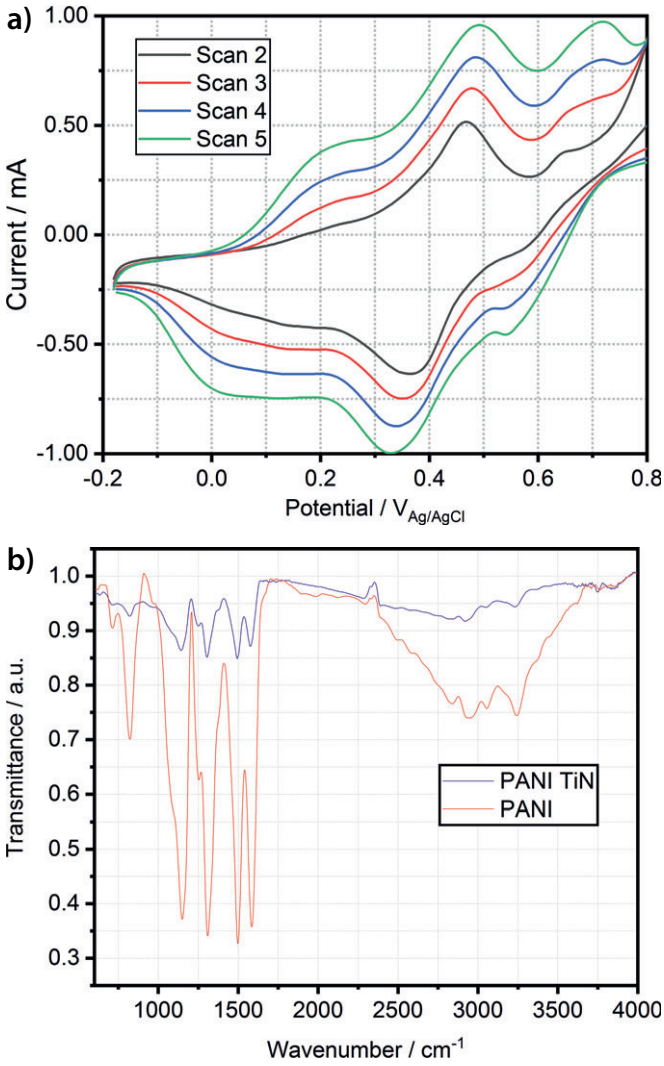


Fig. 1 (a) CV cycle of a 0.1M polyaniline and 0.1 g $L^{-1}$ solution at room temperature (approx. 25 °C). (b) FTIR spectrums of 25 cycle PANI and PANI TiN samples.

to the amount of substance present. By comparing the intensity of the 25 cycle PANI and 25 cycle PANI TiN samples it can be seen that the later has a lower PANI loading, this could mean that the TiN suppresses the polymerization of the aniline onto the surface of the sample, and this would support the mechanism of TiN claiming aniline nucleation sites. This could be due to electrostatic charges being formed on the surface, the dipole present on the TiN could encourage the nanoparticle to deposit at these sites. The peak observed at around 700 $cm^{-1}$ is typically attributed to stretching of the sulfur oxygen double bond [36]. The PANI was polymerized in sulfuric acid which can cause the PANI coating to be doped with sulfate ions. The peaks at 823 $cm^{-1}$ and 1,149 $cm^{-1}$ show the out-of-plane vibration and in-plane vibration of the carbon hydrogen bond; 1,149 $cm^{-1}$ also corresponds to the vibrational mode of the positively charged nitrogen hydrogen structure present in PANI [37, 38]. The shoulder at 1,268 $cm^{-1}$ and peak at 1,309 $cm^{-1}$ correspond to the vibrational modes of the carbon

  

nitrogen bonds. The peak at 1,309 $cm^{-1}$ is a good indicator of the conductivity of the polymer as it corresponds to the π–electron delocalization, it is the extended p-orbital system which allows electrons to move from one end of the system to the other [39].

The peaks observed at 1,500 $cm^{-1}$ and 1,588 $cm^{-1}$ relate to the vibrations of the quinoid and benzoid rings present in the PANI structure. The broadband absorption which can be seen in wavenumbers higher than 2,000 $cm^{-1}$ are typical of PANI in its conducting form.

The bilayer was created by applying a static potential to the metal substrate. EDX measurements have shown that by holding a static potential after the CVs, the TiN loading can be increased and a bilayered coating was formed. Initially up to 300 s the TiN loading stays around the 6% by weight but increasing the time held static to 450 s and 600 s causes the weight % to increase to 8.41%. The TiN 600s sample had a lower weight % than the PANI TiN 600s sample, this confirms the presence of PANI increases the TiN deposition.

### 3.2 *Interfacial Contact Resistance (ICR)*

The ICR of the bare stainless steel, PANI and PANI-TiN coated samples were measured as a function of compression force, as shown in Figure 2. Acid washed bare SS316L had an ICR of 55 mΩ $cm^2$ at 140 N. This is similar to other reported values for SS316L [20]. Polyaniline, although a conducting polymer, has traditionally been problematic in BPP coatings as it greatly increases the contact resistance between the BPP and GDL. Thickness of polyaniline coatings greatly influence the ICR, with thinner coatings having lower ICR values. As previously mentioned, the thickness of the coating can be controlled by the number of cycles, 5 cycles was found to be optimum for ICR in previous work [29]. Coatings were also carried out at 5 °C to reduce the rate of polymerization and create thinner coatings, this value was found to be optimum in our preliminary optimization work. Previous work found the ICR of 5 cycle polyaniline to be 367 mΩ $cm^2$ [29]. This work produced a polyaniline coating with an ICR of 142 mΩ $cm^2$ (quoted values will be for 140N), which is over 50% lower than previously reported values. This reduction of ICR is a result of the lower temperature forming thinner coatings.

Figure 2a shows the comparison of Bare SS and the two polyaniline coatings, it can be seen that the Bare SS out-performs the polyaniline coating even with the reduced thickness of coating. The Bare SS does not have a thick passivation layer at this point, due to the cleaning process employed, and as such has relatively low ICR values.

The polyaniline coating was doped with TiN nanoparticles to reduce the ICR. The introduction of TiN into the polyaniline structure resulted in an ICR of 19.8 mΩ $cm^2$ for the PANI TIN sample. This values almost satisfies the DoE target of 10 mΩ $cm^2$ and again is an improvement upon previous literature, this is due to the thinner coating. It can be seen in Figure 2b that the addition of TiN into the polymer structure reduced the ICR relative to both the bare substrate

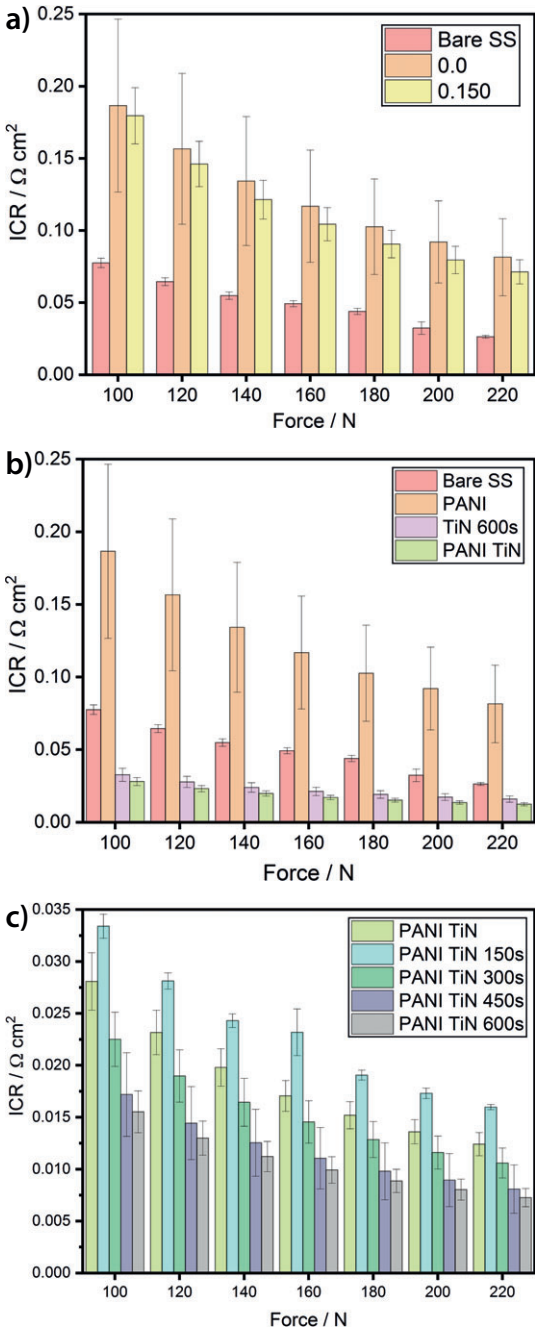


Fig. 2 Interfacial contact resistance measurements for before corrosion, a) Comparison between Bare SS samples and PANI coated samples; b) shows how TiN effects the ICR values, comparing PANI TiN and TiN 600s; c) shows how increasing the time the potential was held at 0.5 V effects the ICR.

and polymer only coating. A sample with a coating of only TiN (TiN 600s) was made, and it was expected that this sample would have a lower ICR than the composite coating but ICR would be greater after corrosion tests. However, it can be seen that the composite PANI TiN coating had a lower ICR even before corrosion tests. It is possible that the PANI could create an increased surface area which also increases the deposition of TiN, due to more nucleation sites

  

being available. Higher surface areas with increased TiN content would result in lower ICR values.

Figure 2c shows the polyaniline and TiN composite coatings, with samples PANI TiN 150s, PANI TiN 300s, PANI TiN 450s, and PANI TiN 600s being the bilayered samples. All bilayer coatings of composite polyaniline TiN with a surface layer of TiN presented lower ICRs than bare, polyaniline and composite layer. Static potentials were held after CV electroplating for 150s, 300s, 450s, and 600s s. ICRs of the bilayers decreased as follows 150s > 300s > 450s > 600s. Interestingly, the PANI TiN 150s sample had a higher ICR than the PANI TiN sample whereas the subsequent samples, PANI TiN 300s, PANI TiN 450s, and PANI TiN 600s, all showed lower ICRs than the composite layer. PANI TiN 600s samples achieved an ICR of 11.2 $m\Omega\,cm^2$. DoE targets are set at 10 $m\Omega\,cm^2$ at a compression of 140 $N\,cm^2$ [4]. The decrease in ICR as the time of static potential held increases is due to the increase in TiN loading at the surface of the sample. 0.5V was held to plate the surface of the coating with TiN, the longer the potential was held the more TiN electrphoretically deposited on the surface. The improved ICR of TiN over polyaniline results in an overall reduced ICR.

### 3.3 Electrochemical Corrosion

Figure 3 shows the potentiodynamic curves obtained in a 1mM (pH 3) sulfuric acid solution at 80 °C saturated with $N_2$. The highest corrosion potential measured was that of the Bare SS sample with a potential of –0.086 $V_{SHE}$. The corrosion potentials observed in this work for the PANI coating, –0.126 $V_{SHE}$, are lower than those observed in other works, where potentials for polyaniline coated samples were in the range of 0.22 $V_{SHE}$ [29]. The thickness of polyaniline coatings have been seen to change the morphology of polyaniline growth. The polyaniline coated samples in that work were thicker than those presented here. It could be possible that there is an optimal thickness for corrosion properties of the sample. The TiN doped PANI coatings increased the corrosion potential with the bilayered sample, PANI TiN 600s, having the highest potential of them all. It is proposed that the TiN blocked pores in the PANI structure, preventing the diffusion of corrosive media to the SS surface, with the bilayer further filling the pores.

The potentiostatic corrosion values are presented in Figure 3. The thin polyaniline coatings all achieved DoE targets with corrosion current densities in the range of ~0.02–0.06 $\mu A\,cm^{-2}$. This suggests that thin polyaniline coatings are an effective barrier to corrosive media, successfully preventing the corrosion of the underlying base substrate. The gold doped PANI coatings investigated in literature [20], showed a corrosion current density of 1.4 $\mu A\,cm^{-2}$. Therefore, it would be expected that TiN doped coatings would outperform the gold doped coatings in long run tests. The improved corrosion resistance relative to other composite polyaniline coatings could be related to the thinner coatings achieved by the reduced electroplating temperature being less porous. The TiN loading is suggested to also increase the density of the coating which could further enhance the corrosion resistance of the substrate. For the composite and bilayered coatings the more time with a static potential after the CVs show a trend of decreasing corrosion current density with increased time. This could be a result of the TiN filling the defects of the polyaniline structure.

BPP's are required to maintain low ICR values, even after exposure to the corrosive environments found in the fuel cell environment. ICR tests were conducted after the corrosion test, to investigate the coatings ability to maintain a low ICR after exposure.

The Bare SS sample increased in ICR to 310 $m\Omega\,cm^2$ highlighting the need for samples to be coated. The PANI sample saw a decrease in ICR to a value of 111 $m\Omega\,cm^2$. This has been seen in previous literature but was reported in thicker 50 cycle coatings [29]. It is possible that the PANI oxidation state was changed during the corrosion test thereby decreasing the contact resistance of the coating.

For the composite coatings the contact resistance increased in both cases. PANI TiN increased from 19.8 $m\Omega\,cm^2$ to 90.3 $m\Omega cm^2$. PANI TiN 600s increased from 11.2 $m\Omega\,cm^2$ to 39.9 $m\Omega\,cm^2$. The TiN 600s showed a large increase in ICR from 24.0 $m\Omega\,cm^2$ to 115 $m\Omega\,cm^2$. The increase in ICR could be due to loss of TiN particles with the corrosion test. The PANI

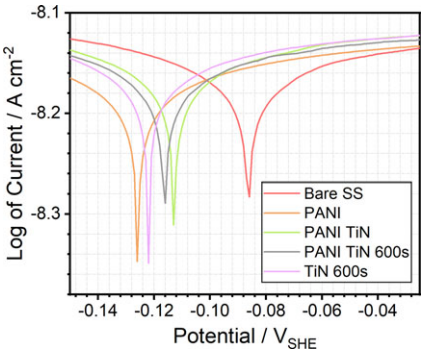


Fig. 3 Linear sweep voltamagrams (LSV) of the different samples (Conditions: pH3 $H_2SO_4$ solution, 80 °C and saturated in $N_2$).

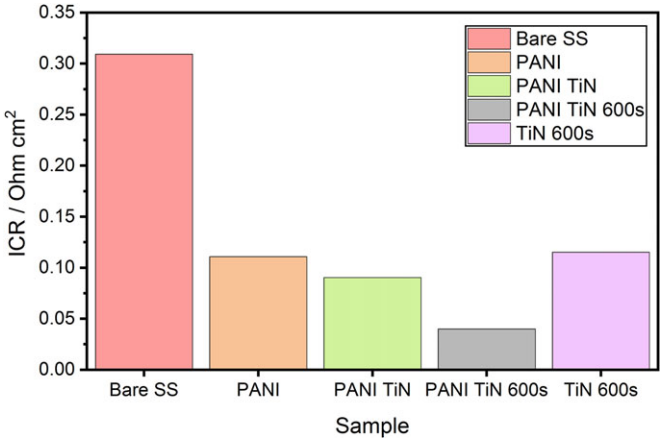


Fig. 4 ICRs of samples after corrosion for 24 h at 80 °C in a pH 3 solution under cathodic conditions (saturated with air, potential 0.9 V).

  

TiN coating with the highest TiN loading showed the lowest ICR before and after corrosion along with the greatest resistance to corrosion.

## 4 Conclusion

A PANI-TiN composite bilayer was developed in a two-step electrochemical process and confirmed by EDX and FTIR studies. It was intended to optimize polyaniline coatings by using: (i) a low temperature for electroplating, (ii) by doping of the polyaniline layer with TiN and by (iii) the addition of a surface layer of TiN to create a bilayered coating. The lower temperature of electroplating effectively reduced the corrosion current density of the layer relative to other works. It also had beneficial results in terms of contact resistance. The doping of the polyaniline layer did not negatively affect the corrosion properties, but improved the contact resistance of the sample. The bilayered structure further reduced the ICR bringing the value closer to the DoE target. One of the barriers to metallic BPP has typically been the high cost of the necessary coatings required. The coating in this work was formed from low cost reactants and plated in a simple two-step process. The best coating in this work PANI TiN 600s achieved corrosion current density requirements of DoE and achieved an ICR of 11 $m\Omega\,cm^2$, this does not quite achieve the 10 $m\Omega\,cm^2$ target of DoE. With further optimization of the surface layer, it is expected that the DoE targets can be achieved with this coating. Future work will investigate the effect of polishing and other pre-treatment processes on the coating and performance of the substrate. The coating characteristics on a formed bipolar plate should also be investigated and its *In situ* performance in PEFC must also be tested.

## Acknowledgements

The authors would like to acknowledge the EPSRC for the funding of the CDT in Fuel Cells and their Fuels, EP/L015749/1, which supported the research conducted in this paper.

## References

[1] *IPCC 2014: Climate Change 2014 – Mitigation of Climate Change*, Working Group III contribution to the Fifth Assessment Report of the Intergovernmental Panel on Climate Change, (Eds: O. Edenhofer, R. Pichs-Madruga, Y. Sokona, E. Farahani, S. Kadner, K. Seyboth, A. Adler, I. Baum, S. Brunner, P. Eickemeier, B. Kriemann, J. Savolainen, S. Schlömer, C. von Stechow, T. Zwickel and J. C. Minx), **2014** Cambridge University Press, Cambridge, United Kingdom und New York, NY, USA.

[2] S. Ali Azimifar, P.h.D. Thesis, University of Birmingham, Birmingham, United Kingdom, **2015**.

[3] C. K. Jin, K. H. Lee, C. G. Kang, *Hydrogen Energy* **2015**, *40*, 6681.

[4] J. Jin, Z. Zhu, D. Zheng, *Hydrogen Energy* **2017**, *42*, 11758.

[5] H. Tsuchiya, O. Kobayashi, *Hydrogen Energy* **2004**, *29*, 985.

[6] R. Taherian, *Power Sources* **2014**, *265*, 370.

[7] N. F. Asri, T. Husaini, A. B. Sulong, E. H. Majlan, W. R. W. Daud, *Hydrogen Energy* **2017**, *42*, 14.

[8] A. G. González-Gutiérrez, M. A. Pech-Canul, G. Chan-Rosado, P. J. Sebastian, *Fuel* **2019**, *235*, 1361.

[9] C. Y. Bai, M. D. Ger, M. S. Wu, *Hydrogen Energy* **2009**, *34*, 6778.

[10] A. Mahdavi, A. A. Ranjbar, M. Rahimi-Esbo, *Applied Energy* **2018**, *228*, 656.

[11] A. Hedayati, S. Asghari, A. H. Alinoori, M. Koosha, E. Vuorinen, *Iranian J. Hydrogen Fuel Cell* **2017**, *3*, 137.

[12] G. Hinds, E. Brightman, *Hydrogen Energy* **2015**, *40*, 2785.

[13] M. Metikoš-Huković, R. Babić, Z. Grubač, Ž. Petrović, N. Lajçi, *Corrosion Science* **2011**, *53*, 2176.

[14] P. Mandal, U. Kumar Chanda, S. Roy, *Materials Today* **2018**, *5*, 17852.

[15] K. McCay, O. E. Kongstein, A. Oedegaard, A. O. Barnett, F. Seland, *Hydrogen Energy* **2018**, *43*, 9006.

[16] C. H. Lin, J. R. Lee, P. J. Teng, S. Y. Tsai, H. H. Sheu, K. H. Hou, M. D. Ger, *Electrochemical Science* **2018**, *13*, 3147.

[17] R. F. Silva, D. Franchi, A. Leone, L. Pilloni, A. Masci, A. Pozio, *Electrochimica Acta* **2006**, *51*, 3592.

[18] B. Navinšek, P. Panjan, I. Milošev, *Surface Coatings Technology* **1999**, *116*, 476.

[19] K. Zhang, S. Sharma, *ACS Sustainable Chemistry Engineering* **2017**, *5*, 277.

[20] S. Pugal Mani, A. Srinivasan, N. Rajendran, *Hydrogen Energy* **2015**, *40*, 3359.

[21] M. Omrani, M. Habibi, M. S. Moti Birjandi, *Hydrogen Energy* **2016**, *41*, 5028.

[22] S. Wan, M. Hou, Q. Zhou, Y. Jiang, Z. Wang, H. Li, Y. Fu, Z. Shao, *Energy Chemistry* **2017**, *26*, 168.

[23] Y. Fu, M. Hou, G. Lin, J. Hou, Z. Shao, B. Yi, *Power Sources* **2008**, *176*, 282.

[24] M. Kumagai, S. T. Myung, R. Asaishi, Y. K. Sun, H. Yashiro, *Electrochimica Acta* **2008**, *54*, 574.

[25] V. S. Bhadram, H. Liu, E. Xu, T. Li, V. B. Prakapenka, R. Hrubiak, S. Lany, T. A. Strobel, *Physical Review Materials* **2018**, *2*, 11602.

[26] S. Zhang, W. Zhu, *Material Processing Technology* **1993**, *39*, 165.

[27] T. J. Pan, X. W. Zuo, T. Wang, J. Hu, Z. D. Chen, Y. J. Ren, *Power Sources* **2016**, *302*, 180.

[28] R. M. Bandeira, J. van Drunen, A. C. Garcia, G. Tremiliosi-Filho, *Electrochimica Acta* **2017**, *240*, 215.

[29] S. Sharma, K. Zhang, G. Gupta, D. G. Santamaria, *Energies* **2017**, *10*, 1152.

[30] S. Joseph, J. C. Mcclure, R. Chianelli, P. Pich, P. J. Sebastian, *Hydrogen Energy* **2005**, *30*, 1339.

[31] S. Joseph, J. C. Mcclure, P. J. Sebastian, J. Moreira, E. Valenzuela, *Power Sources* **2008**, *177*, 161.

[32] M. A. Deyab, *Power Sources* **2014**, *268*, 50.

  

[33] K. Zhang, Master Thesis, University of Birmingham, Birmingham, United Kingdom, **2016**.
[34] K. Huang, Y. Zhang, Y. Long, J. Yuan, D. Han, Z. Wang, L. Niu, Z. Chen, *Chemistry a European Journal* **2006**, *12*, 5314.
[35] A. El-Kharouf, T. J. Mason, D. J. L. Brett, B. G. Pollet, *Power Sources* **2012**, *218*, 393.
[36] K. Pekmez, *Synthetic Metals* **2002**, *131*, 7.
[37] S. Quillard, G. Louarn, J. P. Buisson, M. Boyer, M. Lapowski, A. Pron, S. Lefrant, *Synthetic Materials* **1997**, *84*, 805.
[38] M. Trchova, I. Sedenkova, E. Tobolkova, J. Stejskal, *Polymer Degradation and Stability* **2004**, *86*, 179.
[39] K. M. Molapo, P. M. Ndangili, R. F. Ajayi, G. Mbambisa, S. M. Mailu, N. Njomo, M. Masikini, P. Baker, E. I. Iwuoha, *Electrochemical Science* **2012**, *7*, 11859.

  